$2^{-\rho}$

NASA TECHNICAL NOTE

NASA TN D-7679
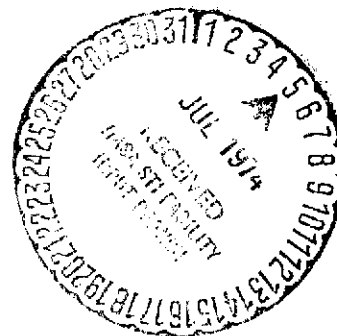
ATMOSPHERIC TEMPERATURE
MEASUREMENTS USING RAMAN LIDAR

by Jack A. Salzman and Thom A. Coney

Lewis Research Center

Cleveland. Ohio 44135

NATIONAL AERONAUTICS AND SPACE ADMINISTRATION • WASHINGTON, D. C. • JUNE 1974

27

1. Report No. NASA TN D-7679	2. Government Accession No.	3. Recipient's Catalog No.
4. Title and Subtitle ATMOSPHERIC TEMPERATURE MEASUREMENTS USING RAMAN LIDAR		5. Report Date June 1974
		6. Performing Organization Code
7. Author(s) Jack A. Salzman and Thom A. Coney		8. Performing Organization Report No. E-7874
		10. Work Unit No. 501-04
9. Performing Organization Name and Address Lewis Research Center National Aeronautics and Space Administration Cleveland, Ohio 44135		11. Contract or Grant No.
		13. Type of Report and Period Covered Technical Note
12. Sponsoring Agency Name and Address National Aeronautics and Space Administration Washington, D.C. 20546		
		14. Sponsoring Agency Code

15. Supplementary Notes

16. Abstract

The Raman-shifted return of a lidar system has been used to make atmospheric temperature measurements. The measurements were made along a horizontal path at temperatures ranging from -30° to 30° C and at ranges of about 100 meters. The temperature data were acquired by recording the intensity ratio of two portions of the rotational Raman spectrum, which were simultaneously sampled from a preset range. These tests verified that the theoretical predictions formulated in the design of the system were adequate. Measurements were made to an accuracy of ±4° C with 1-minute temporal resolution.

17. Key Words (Suggested by Author(s)) Optical radar Raman spectra Temperature measuring instruments	18. Distribution Statement Unclassified - unlimited Category 16

19. Security Classif. (of this report) Unclassified	20. Security Classif. (of this page) Unclassified	21. No. of Pages 25	22. Price* $3.00

ATMOSPHERIC TEMPERATURE MEASUREMENTS USING RAMAN LIDAR

by Jack A. Salzman and Thom A. Coney

Lewis Research Center

SUMMARY

Experiments were conducted to demonstrate that the Raman-shifted return of a lidar system can be used to remotely measure atmospheric temperature. The measurement technique involves simultaneously monitoring the intensities of two portions of the Raman signal sampled from a preset range and examining the ratio of their intensities. A theoretical analysis relating the ratio of the Raman spectral intensities transmitted by a variety of interference filter pairs was performed to establish a predicted temperature measurement sensitivity. Experimental data were obtained at a horizontal range of about 100 meters for ambient air temperatures ranging from -10° to 22° C during both daylight and night time hours.

Data were also obtained using a 12-meter-long volume of temperature-controlled air. The temperature within the zone was varied from 25° C below to 15° C above the ambient air temperature. These tests indicate that 10 shots, or 1 minute of data acquisition, can provide absolute temperature measurements with an accuracy of $\pm 4^\circ$ C at a distance of 100 meters. The theoretical and experimental results compared favorably, and system capabilities were near those predicted for the particular unit tested.

INTRODUCTION

Lidar systems are presently being used on an experimental scale to measure a wide variety of meteorological variables. A number of investigators are regularly observing elastically backscattered light to remotely measure atmosphere modeling parameters such as aerosol and particulate distributions (refs. 1 to 5). Others have investigated the incorporation of lidar techniques with inelastic Raman scattering to measure atmospheric temperature (ref. 6) and constituent and pollution levels (refs. 7 to 11). A method of using Raman scattering for temperature measurements, which was suggested for use in atmospheric probing (ref. 12), has been shown to be feasible in the laboratory (refs. 13 to 15). The technique involves the examination of the ratio of the measured

intensities of at least two portions of the Raman scattered signal from the atmosphere.

The purpose of this project was to demonstrate the feasibility of using the technique, integrated with a lidar system, to make remote measurements of atmospheric temperature. To achieve this purpose a lidar system was constructed at the Lewis Research Center (ref. 16). The lidar system was designed to simultaneously sample two portions of the Raman spectrum from a preset range through the use of a beam splitter and two interference filters. Because a major problem in past lidar studies has been the lack of calibrated baseline measurements, a test range was also constructed wherein the temperature of a large volume of air could be controlled and monitored. The test range had a total horizontal path length of 200 meters with the target volume located 100 meters from the lidar unit. The temperature of the air in the target volume could be raised or lowered with respect to the temperature of the ambient air.

This report presents a discussion of measurement theory, instrumentation, procedure, and resulting experimental data. Included is a direct comparison of the theoretical and experimental results. The experimental data were obtained at ambient air temperatures ranging from -11° to 22° C and at controlled air temperatures ranging from -30° to 30° C.

THEORY OF MEASUREMENT TECHNIQUE

Background

Fundamental Raman theory is well documented. Using that theory and considering only the contributions from the oxygen and nitrogen components of air, Coney and Salzman (ref. 13) modeled the Raman rotational spectrum of air. The relative line intensities, positions, and shapes of the model compared well with experimental spectra. The theoretical equations used to obtain the model related the rotational spectral intensity to the temperature of the air producing the spectrum. This temperature dependence is demonstrated in figure 1 in which two rotational spectra of air are shown, one calculated assuming an air temperature of 243 K and the other an air temperature of 313 K. For illustrative purposes the spectra shown in figure 1 were calculated to represent the throughput of a monochromator with a slit width near 2 inverse centimeters (ref. 13). Note that the actual Raman line widths before instrument distortion are approximately 10 percent of those shown.

Figure 1 also illustrates that a measure of the spectral line intensities can be a measure of the temperature of the air. This was shown in the laboratory to be the case (refs. 13 to 15). With only slight variation, this is the measurement technique used in this study.

As previously stated, the purpose of this study was to use this technique in a field demonstration of a lidar unit to remotely measure air temperature. Because the amount of light inelastically scattered from a remote sample of air is very small, interference filters with their comparatively high light gathering capabilities and large apertures were used to achieve wavelength selection. Thus, spectral band intensities, rather than spectral line intensities, were measured, resulting in a maximization of return signal statistics. To insure that the temperature measurement was independent of varying atmospheric transmission and electronic response characteristics, the transmitted intensities of two different spectral bands were simultaneously measured and their ratio related to the air temperature. Since the difference between the center wavelengths of any two bands in the rotational spectrum is small, the uncalibrated atmospheric and electronic effects, to a good approximation, have the same effect on both band intensities. By taking their ratio, these effects are canceled. The simultaneity of the dual measurement resulted in high temporal resolution and made real-time temperature measurements possible.

Selection of Spectral Bands

The specific spectral bands (denoted by interference filter center wavelength and bandwidth) to be used in the temperature measurement were chosen through an analysis of the sensitivity of the band intensities to changes in temperature and through an analysis of the system statistics. This analysis could be most simply accomplished by assuming the filter transmittances as a function of wavelength to be Gaussian shaped and by approximating the broadened Raman spectrum by an ideal line spectrum. A comparison of the measured transmittance of a filter and a Gaussian curve fitted to it (fig. 2) showed the assumption to be justified. Using a Gaussian filter transmittance, a comparison of band intensities calculated with an actual Raman spectrum having finite bandwidths and with a simpler line spectrum showed such an approximation also to be adequate.

The most desirable spectral band or filter combination is that resulting in the lowest standard deviation of the temperature. Reference 17 showed the standard deviation to be given by the equation

$$\Delta T = \frac{1}{slope} \left[\frac{I_J(I_J + I_K)}{I_K^3} \right]^{1/2} \tag{1}$$

where the slope is simply

$$\text{slope} = \frac{\dfrac{I_J(T_1)}{I_K(T_1)} - \dfrac{I_J(T_2)}{I_K(T_2)}}{T_1 - T_2} \tag{2}$$

and where I_J and I_K are the total of the dimensionless Raman line intensities trans-
mitted through the J and K filter bands and are directly related to the lidar return
signal, and T_1 and T_2 are two different air temperatures. To obtain the filter com-
bination producing the minimum ΔT, all possible band combinations must be considered.
This was accomplished, within practical limits, by calculating total band intensities at
each of two air temperatures near 253 K for filter center wavelengths ranging from
686.6 to 702.2 nanometers in 0.2-nanometer increments. The bandwidths at each of the
center wavelengths ranged from 0.4 to 3.8 nanometers in 0.2-nanometer increments.
The total Raman return signal detected was assumed to be about 10^4 photons. All the
resulting band intensities were appropriately substituted into equation (1). Four spec-
tral band combinations produced relative minima in the standard deviation. Table I
lists these combinations using the notation 687.6-2.4, where the center wavelength is
687.6 nanometers and the bandwidth is 2.4 nanometers. (This notation is used through-
out the remainder of the report.) The absolute values of the standard deviations pre-
sented were obtained through a normalization process based on an estimated Raman sig-
nal return and assuming typical lidar system efficiencies. The existence of four minima
can be accounted for by noting the spectral behavior as a function of temperature in the
four regions (A to D) in figure 1. In regions A and D the spectral intensity decreases
with an increase in temperature. In regions B and C the spectral intensity increases
with an increase in temperature. Therefore, the ratio of an increasing region either B
or C with a decreasing region either A or D will result in an enhanced variation with
temperature.

These results, which indicate the ideal filter combinations to be used to measure air
temperature, must be weighted by practical limitations associated with the use of inter-
ference filters. A very significant limitation is a consequence of the dependence of the
filter transmittance on the incident angle of the light being filtered. Because the trans-
mittance curve "shifts" toward the shorter wavelength as a function of the deviation of
that angle from the normal (ref. 18), the blocking of the laser line by a thin film inter-
ference filter designed to transmit in the Stokes spectrum may be effectively degraded
if the incident light can reach the filter at some high angle of incidence. Because of the
relatively high intensity of the Rayleigh-Mie return, multiple reflections leading to that
situation are highly probable. In fact, this type of leakage was noted experimentally.

A second disadvantage in using filters transmitting in the Stokes spectrum becomes
evident when consideration is given to the fluorescence spectrum. Since fluorescence
results in scattered light having for the most part wavelengths greater than the source

4

(i.e., the laser wavelength), the total light intensity transmitted by a Stokes filter may include a component scattered by fluorescence in addition to that scattered by the Raman process. Therefore, to minimize any difficulties associated with the angle dependence of the filters and to avoid the inclusion of fluorescent light, filters transmitting in the Stokes spectrum were not considered for use in the remote temperature measurement. Thus, the theoretical combination most practically suitable for making the temperature measurement is that using the 687.8-2.6 and 692.6-0.8 filters (table I).

The final filter selection rests on the availability of filters having the desired transmittance as well as having sufficient blocking outside the bandpass region (i.e., at least 10^{-5} rejection at the laser wavelength). No difficulty was anticipated in obtaining the broadband filter. However, a 692.6-0.8 filter could not be found with an acceptable laser line rejection or blocking. To insure the desired rejection, the narrow band filter was shifted away from the laser line. The combination finally used to make the temperature measurement consisted of a 691.3-0.4 and 687.4-2.4 filter pair. The standard deviation of a temperature measurement made with this filter pair was predicted to be 12.5 K.

Ratio Variation with Air Temperature

Having established the two spectral bands to be used in making the temperature measurement, it is possible to calculate the variation of their ratio as a function of air temperature for the proposed measurement system (ref. 13). This variation is shown in figure 3 for the 691.3-0.4 and 687.4-2.4 filter combination.

Small temporary or permanent changes can occur in the filter transmittances as a consequence of fluctuations in filter temperature and of the normal aging process of filters. The effect of these potential changes on predicted correlations such as shown in figure 3 must be evaluated to accurately relate experimental data to this correlation. Figure 4 shows the intensity ratio - temperature curves calculated using filter combinations having transmittance characteristics slightly different from those specified. A comparison of these curves indicates that significant variations in the magnitude of the ratios can occur for only minor filter value changes. Consequently, such changes could result in serious errors in the measurement of absolute temperature and should be considered in the evaluation and design of the measuring system.

The impact of filter value changes on relative temperature measurements is not as significant if a normalization process is used in the system calibration procedures. First, a calibration curve for the actual system can be obtained by matching a theoretical curve such as those in figure 4 to a range of experimental data. (The data must have been obtained using a single filter pair under conditions assuring no shift in the trans-

mittance characteristics of the filters.) Then subsequent temperature measurements can be made using only one ratio measurement at a known temperature to establish an interim reference calibration point. This point can be normalized to the system calibration curve and associated ratio measurements at unknown temperatures, corrected by the resulting normalization factor. This procedure is illustrated in figure 5. Shown are the two curves in figure 4 that represent the extremes of ratio magnitudes normalized to the 691.3-0.4 - 687.4-2.4 calibration value at a temperature of -10° C.

Even though filter extremes were used in figure 5, the temperature sensitivity (i.e., slope) of the three filter pairs are only slightly different. The maximum temperature measurement discrepancy associated with these shifted transmittances is about 5 K after normalization. In addition, this error can be considerably reduced if the reference or normalizing measurement is made at a temperature near the unknown temperature.

The relative constancy of the temperature sensitivity can be explained by noting that the narrow band filter is transmitting in a region of the spectrum that changes only slightly with air temperature, while the broadband filter is transmitting in a region in which the change is nearly constant. Therefore, slight shifts in filter transmittance affect ratio magnitude but not temperature sensitivity.

APPARATUS AND PROCEDURE

Test Facility

To evaluate the potential of the measurement technique and to acquire field test data with the Raman lidar unit, a test range was constructed at the Lewis Research Center. This test range encompasses a total horizontal path length of 200 meters and consists of the three major components shown in figure 6. A 2.2- by 7.5-meter trailer houses the basic lidar system, associated alinement gear, and other test and control equipment. Located 100 meters from the trailer is a control zone, which contains a test volume of air, the temperature of which can be either raised or lowered with respect to the ambient outside temperature. Located 200 meters from the trailer is an energy dump and safety shield which terminates the laser beam's path and satisfies other safety requirements.

An interior view of the lidar trailer is shown in figure 7 locating the various control and electronic assemblies. All the test operations are controlled from this trailer compartment, and all range personnel remain in this area during testing. The laser and receiving telescope are separated from this compartment by an opaque wall for safety and for the isolation of the detected light from normal trailer lighting. A small hatch positioned in the front of the trailer allows the laser light pulse to leave and the scattered

light to enter. The entire trailer is stabilized through a hard mounting system.

The control zone shown in figure 8 is 2.4 meters in diameter and 12 meters long. With the end doors closed the temperature of the air inside can be raised through the use of infrared heaters or cooled through the use of a liquid-nitrogen heat exchanger and circulation system. The limits on the attainable difference between zone and ambient air temperatures were +15° and -25° C. The maximum positive temperature difference is due simply to a limitation of heater power. The maximum negative temperature difference is dictated by the increasing potential for condensation or fog generation at larger differences. A series of thermocouple rakes is used to continuously monitor the air temperature. When the desired air temperature is reached, the hinged doors at each end of the zone are remotely opened for testing. A 0.6-meter wide collar is positioned at each end of the zone (visible in fig. 8) to restrict air flow in or out of the zone. This collar then provides a 1.2-meter diameter aperture through which the laser pulse can enter and leave the control zone.

After traversing the control zone, the path of the laser pulse is terminated at the energy dump (fig. 9). To prevent high intensity reflection, both for the protection of area personnel and the detection electronics, the energy dump is constructed from a double row of light absorbing cones set in a 1.2-meter-square array. This energy dump is then backed by a large flat black screen (fig. 9) to prevent any laser light around the perimeter of the beam from proceeding down range.

Raman Lidar Unit

A schematic of the optical design of the lidar unit is shown in figure 10. The transmitter, which supplies the incident light, is a Q-switched ruby laser operating with an output wavelength of 694.3 nanometers. The output pulse width is 20 nanoseconds (6-m long), and the output energy is 4 joules per pulse at the rate of 10 pulses per minute. The relative energy from each pulse is monitored with a photodiode detector and storage oscilloscope. The light scattered from the pulse as it passes through the atmosphere is collected by an f/13 Schmidt-Cassegrain telescope 25.4 centimeters in diameter. Because of the short ranges involved in this testing, the optical axis of this telescope is alined to intersect the path of the light pulse at a range of 100 meters. This requires that they converge at an angle of about 8 minutes.

Light collected by the telescope is passed to an optics box where it is first split into two components by a pellicle beam splitter with each component then going to a filter-PMT (photomultiplier tube) assembly. In the wavelength region of concern in this study (i.e., near 700 nm) the beam splitter reflects 27 and 73 percent, respectively, of the polarized and unpolarized components of the return light. The filter-detector

assemblies (i.e., filter 1 - PMT 1 and filter 2 - PMT 2 in fig. 10) supply the Raman intensity data used in the temperature measurement. The temperature of these filters is controlled through use of a liquid circulation system in order to maintain constant their transmission characteristics during a test series. The relative gain of the PMT's can be periodically checked using a light emitting diode-fiber optic unit. A portion of the combination Rayleigh-Mie scattered light at 694.3 nanometers, which is rejected and, thus, partially reflected by filters 1 and 2, is monitored using the filter 3 - PMT 3 assembly.

The signal outputs of the three filter-PMT assemblies are sent to an electronics unit for processing and display (fig. 11). The Rayleigh-Mie signal is simply displayed on an oscilloscope and recorded on polaroid film. The Raman signals are also sent to an oscilloscope display, but, in addition, they are processed for a more accurate read-out and storage. A fixed segment (normally 20 to 80 nsec) of the total return signal is sampled during each test. The relative time at which this sample is taken after the laser firing determines the range from which the scattered light is being detected. The time or range at which the sample is taken can be continuously adjusted from about 80 to 200 meters. The signal is sampled and gated using a standard nuclear instrumentation module called a "linear gate and hold" by its manufacturer. This gate has a 100-megahertz analog bandwidth and a combined gate opening and closing time of 5 nanoseconds. The gate output is integrated and held such that the magnitude of the output is a linear function of the integral of the signal during the gate opening. Because the output is held for 500 microseconds, it can be digitized by moderate-speed commercial analog-to-digital converters for display on a light-emitting-diode numeric array and for storage on printed tape. A more detailed description of these detection electronics can be found in reference 16.

Test Procedures

Before actual testing, a normal warmup period of about 30 minutes was required to establish the correct filter and PMT temperatures and to stabilize drift in the detection electronics. This time was used to prepare the test range for firing and to aline the laser and telescope units. Through the use of a small continuous wave laser and auto-collimation techniques, it was possible to precisely determine the output path of the ruby laser. This laser output was then alined along the centerline of the test range, and a light was positioned in its path 100 meters downrange. This point also coincided with the center of the control zone. The direction and focus of the telescope was adjusted until its image of the alinement light was positioned along the centerline of the filter-PMT assemblies and the image-plane was at the cathode surface of the PMT's. Because large

variations were noted in the quantum efficiency of the photocathode as an image was scanned across it, this alinement procedure was very critical to the acquisition of repeatable data.

After the detection electronics were fully warmed up, a series of known currents were fed into the first stage amplifiers of each Raman channel, and their components were balanced to provide identical gain characteristics and outputs. Although similar attempts were made to equalize the gains of the two Raman PMT's by adjusting their bias voltages, an exact balance could never be achieved or maintained without great care and effort. Because of this difficulty, the established procedure was to measure the gain difference of the PMT's (normally less than 10 percent) before testing and then monitor the relative gains continuously during testing. This gain factor could then be applied to the data to yield a true Raman signal intensity ratio for each test.

Final adjustments of the detection electronics involved setting the various sequence times such as the PMT gate-on time, PMT gate-off time, and the signal sample time. The original electronics design (ref. 16) employed a laser light pulse detector for time synchronization. Problems were encountered with this scheme when it was used in combination with PMT gain-gating. If the PMT's were left gated off for more that 200 nanoseconds after the laser was fired, an afterpulse was emitted from the PMT's. (Afterpulsing has been noted by other investigators. See refs. 19 and 20.) This problem, together with an inherent switching delay in the gating circuitry of about 200 nanoseconds, required that a time synchronization input be supplied to the gating trigger before the actual laser firing. This requirement was met by the use of a pulse from the Q-switch thyratron circuitry. All time sequences were subsequently set from this base time and, therefore, it was important that the jitter of the laser output be small. It was established that, if the actual laser firing followed two flashlamp firings, the output jitter for all following shots was less than 10 nanoseconds. All test series were, therefore, preceded by a flashlamp firing sequence.

After a test series was initiated and signals were received on both the Raman channels and the Rayleigh-Mie channel, another system check was made prior to data acquisition. One of the primary concerns in the operation of the system was that the signal in each temperature data channel was a pure Raman signal and did not contain signals attributable to scattered light at the exciting laser wavelength (694.3 nm). To determine this, first a shutter on the optics box was closed to establish a null signal condition on all channels. Then a narrow band interference filter with a passband centered at 694.3 nanometers was placed in front of the optics box, and the shutter was opened. Under these conditions, the Rayleigh-Mie signal returned to about 50 percent of its original value while neither of the Raman channels indicated any signal above the null baseline. This result was taken as evidence that the Raman filters provided sufficient blocking of the 694.3-nanometer return signal and that Raman data acquisition could proceed.

If the signal outputs of the three filter-PMT assemblies are displayed on an oscillo-scope, the resulting voltage traces are as shown in figure 12. The waveforms repre-sented in this figure were traced from high-speed polaroid photographs and, therefore, are representative of the shapes and signal-to-noise ratios that were actually received. The vertical scales of the two Raman channels are the same, and their intensities can be compared directly. The intensity scale of the Rayleigh-Mie channel, however, is arbi-trary because of the secondary nature of its signal acquisition. Only qualitative meas-urements are made with this signal. The actual Rayleigh-Mie scattered light intensity is at least three orders of magnitude greater than the Raman intensity.

In each of the traces in figure 12, at time or range equal to zero, the light pulse leaves the laser, and the intensity level is that of the electrical baseline. Tests were conducted during both daylight and nighttime hours, and in all cases the background level due to ambient light intensities was within the noise level of the system. This complete lack of background ambient light can be attributed in part to the horizontal beam path and the terminating energy dump. No tests were made to evaluate the effects of these con-straints. After the light pulse leaves the laser, the received signal starts to increase until it reaches a maximum near that range where the beam path is fully within the field-of-view of the receiver telescope. After the full-on point the mean return signal de-creases as the inverse square of the range. The increased signal at a range of 200 meters represents a reflection from the energy dump. The large variations near the beginning of the signal trace are due to electrical noise generated in the laser Q-switch circuitry. Although great care was taken to shield all system components, these noise fluctuations could not be reduced below that shown in the typical traces of figure 12. Fortunately, these fluctuations damped out rapidly, and their amplitude near the 100-meter range was well below that due to normal light scattering and PMT statistics.

The magnitude of the Raman return signals as shown in figure 12 agree well with values calculated using standard lidar formulas (e.g., ref. 20). Sample calculations were made as a function of range for the signal expected through a 30-percent transmit-tance interference filter with a passband centered at 691.4 nanometers and a bandwidth of 0.4 nanometer. The absolute rotational Raman cross section values used in the cal-culations were obtained from reference 21. These values were 3.55×10^{-30} and 8.40×10^{-30} square centimeter per steradian for nitrogen and oxygen, respectively. When applying an exciting laser energy of 4 joules and incorporating other system pa-rameters such as manufacturer supplied PMT characteristics, the calculated signal re-turn near a 100-meter range is on the order of 30 milliamperes of PMT anode current. The actual signal return was normally 5 to 10 milliamperes before amplification.

Cursory measurements of the return signal polarization characteristics also com-pared well with theoretical predictions. The measured depolarization ratio of the return

10

signal from clean air at 694.3 nanometers (i.e., Rayleigh-Mie signal) was approximately 0.10, which is common for an urban environment (ref. 4). This would indicate that between 15 and 20 percent of the nonshifted return was from asymmetrical scattering elements. The depolarization ratio of the Raman scattered return was 0.68 as compared with the theoretical value of 0.75 for pure air.

After the full-on point, the ratio of the intensities of the two Raman channels (fig. 12) at any particular range is a direct indication of the atmospheric temperature at that range. Although traces such as these could be used to make quantitative temperature measurements and perhaps also to determine temperature gradient locations, the accuracy of this data reduction procedure is severely limited. And, when using standard manual techniques, the data acquisition rate is slow. For these reasons all data used in the temperature analysis was acquired in digital form on printed tape. The data recorded for each test shot included a received signal intensity, a background intensity, and a balance check intensity for both Raman channels. A Raman intensity ratio was calculated by first subtracting the background signal from the received signal, taking the ratio of that quantity, and then correcting this ratio, if necessary, by a gain factor obtained from the balance test.

When a 20-nanosecond sample time was used, the typical one-sigma deviation of the Raman intensity ratio was 10 percent. This error in the ratio measurement could be reduced at a loss of temporal resolution by averaging over several test shots or at a loss of spatial reduction by increasing the sample time. For example, by increasing the sample time to 48 nanoseconds, the deviation was actually reduced to only 6 percent. As a compromise, all intensity ratio data discussed in the remainder of this report were acquired with a sample time of 20 nanoseconds, but each data point represents the arithmetic average of 10 test shots or one minute of test time.

Temperature measurement data obtained in this digital format is shown in figure 13 where the measured Raman intensity ratio is plotted as a function of the ambient atmospheric temperature. The control capabilities of the control zone were not used for these tests. These data samples were taken at ranges varying from about 100 to 120 meters during the winter when the ambient temperature was in the range from -10° to 15° C.

The line shown in figure 13 represents a weighted least mean square fit to the data. This fit was obtained from theoretical calculations by finely adjusting the filter characteristics about their measured values until a minimum deviation from the data was obtained. The transmittance characteristics of the two filters used to calculate the line in figure 13 were 691.2-0.4 and 687.4-2.05 with peak transmittances of 30.5 and 26 percent, respectively. The one-sigma deviation of the data from this calculated line was $\pm 4^\circ$ C.

With this correlation of intensity ratio response to temperature variations determined, additional tests were conducted using the control zone to create a target volume

of air whose temperature was substantially different from the ambient outside temperature. The mean zone air temperature for the series ranged from 15° C above ambient to 25° C below ambient. For these tests the sample range was centered in the control zone (i.e., 100 m). Figure 14 shows the results of these tests where, again, each data point represents 10 consecutive test shots. The line drawn through the data is the established correlation from figure 13. In general, the greatest error from the predicted behavior was at the low-temperature extreme of the data where the Raman intensity ratios were lower than predicted. This would result in higher indicated Raman temperature than that measured by thermocouples. This discrepancy is also illustrated in figure 15 where data from the same test series is presented in another format.

The data as plotted in figure 15 illustrate that an increase or decrease in zone temperature was always appropriately indicated. However, the magnitude of the change in the cooled zone was less than expected. This could be because the differential between the sampled air volume temperature, which was measured by thermocouple probes, and the ambient air temperature was really not as large as implied. The actual temperatures of the air inside the zone could normally only be determined to within about 5° C before the test shots because of uneven heating or cooling and thermal stratification and to within about 8° C after the test shots because of the migration of ambient air into the zone. This was a particular problem with a large cooled zone. Also, any error in establishing the range at which the sample was taken would cause a deviation in the temperature of the sampled volume toward ambient. Even with these problems, the results shown in figures 14 and 15 do indicate that the temperature of a layer of air as little as 12 meters thick can be measured with this system.

During the completion of the control zone test series, a significant inconsistency was noted in the intensity ratio data. At the beginning of one day's testing, intensity ratios were consistently below those predicted for a particular temperature. Because this downward shift in the intensity ratio persisted, a short test series was conducted for comparison with the previous ambient data. The data obtained in the second ambient series is shown in figure 16 along with the primary data fit correlation from figure 13. The shifted data fit line shown in figure 16 was obtained again from the theoretical calculation but this time by adjusting the filter characteristics about those values used to calculate the primary data fit line. The downward shift in the data fit (fig. 16) can be achieved by any combination of a few nanometers shift in the center wavelength or bandwidth of either filter or a less than 5-percent change in either of their peak transmittances. Unfortunately, during an attempt to determine the exact cause of this shift through a remeasurement of this filter characteristics, one of the filters was permanently damaged, and no conclusive results were obtained.

The data of figure 16 illustrate the major difficulty remaining in using such a system to make absolute temperature measurements. The unpredictable behavior of interference filters such as those used in this study require that repeated calibration tests be

made to check the intensity ratio value at a particular temperature. However, as discussed in the section Theory of Measurement Technique, once this value is determined, at one temperature, its value at any other temperature can easily be extrapolated through a normalization procedure. Also, even if an absolute measurement cannot be acquired, relative temperature measurement such as lapse rate and gradient conditions can still be obtained accurately.

When the one filter from the original filtering combination was damaged, its replacement with another filter required a new system calibration. This calibration or data fit correlation is shown in figure 17. Although data were obtained at only two temperatures, these were considered adequate because of the good correlation data fits that were obtained with the original filter combination. In fact, calibration data for only one temperature is needed for such a correlation. Data for the second set of temperatures were obtained as a final check on the system.

CONCLUSIONS

The purpose of this study was to demonstrate that the Raman-shifted return of a lidar system could be used to make remote atmospheric temperature measurements. After the development and construction of a Raman lidar system, test measurements were made along a horizontal path at temperatures between -30° and 30° C and at ranges of about 100 meters. Temperature data were acquired by recording the intensity ratio of two portions of the Raman spectrum that were simultaneously sampled from a preset range. Tests initially conducted at ambient conditions using the normal outside air temperatures as a test parameter provided a correlation of the Raman intensity ratio as a function of temperature for the particular optical-filter arrangement used in the system. These tests verified that the theoretical predictions formulated in the design of the system were adequate. Tests were also conducted with controlled temperatures above and below ambient to provide temperature gradient data.

The results of these tests indicate (1) that 10 shots, or 1 minute of data acquisition, from a 100-meter range with the present system, can provide absolute temperature measurements with an accuracy of $\pm4^\circ$ C and a range resolution of about 12 meters, (2) that the small fluctuations in transmittance inherent with narrow-band interference filters can be accounted for through a single-point calibration and a normalization procedure, and (3) that, because the measurement accuracy compares well with that predicted for the particular unit tested, a field-application system can be built with significant improvements in both measurement accuracy and range.

Lewis Research Center,
    National Aeronautics and Space Administration,
        Cleveland, Ohio, March 14, 1974,
            501-04.

REFERENCES

1. Grams, G. W.; and Wyman, C. M.: Compact Laser Radar for Remote Atmospheric Probing. J. Appl. Meteorology, vol. 11, Oct. 1972, pp. 1108-1113.

2. Herman, Benjamin M.; Browning, Samuel R.; and Reagon, John A.: Determination of Aerosol Size Distributions from Lidar Measurements. J. Atmos. Sci., vol. 28, no. 5, July 1971, pp. 763-771.

3. Schotland, R. M.; Sassen, K.; and Stone, R.: Observations by Lidar of Linear Depolarization Ratios for Hydrometeors. J. Appl. Meteorology, vol. 10, Oct. 1971, pp. 1011-1017.

4. Pal, S. R.; and Carswell, A. I.: Polarization Properties of Lidar Backscattering from Clouds. Appl. Opt., vol. 12, July 1973, pp. 1530-1535.

5. Collis, R. T. H.; Viezee, W.; Hake, R. D., Jr.; and Russell, P. B.: Lidar Measurements of the Variability of Stratospheric Particulates. Paper 73-520, AIAA, June 1973.

6. Strauch, R. G.; Derr, V. E.; and Cupp, R. E.: Atmospheric Temperature Measurement Using Raman Backscatter. Appl. Opt., vol. 10, no. 12, Dec. 1971, pp. 2665-2669.

7. Jyumonji, M.; Kobayasi, T.; and Inaba, H.: Measurement of Resonance Scattering Cross Section of Sodium D Lines and Laser Radar Detection of Sodium Layer in the Upper Atmosphere by a Tunable Dye Laser. Presented at Fifth Conference on Laser Radar Studies of the Atmosphere (Williamsburg, Va.), June 1973.

8. Strauch, R. G.; Derr, V. E.; and Cupp, R. E.: Atmospheric Water Vapor Measurement by Raman Lidar. Remote Sensing of Environment, vol. 2, Feb. 1972, pp. 101-108.

9. Schildraut, E. Robert: Pollution Analysis Using Remote Raman Spectroscopy. American Laboratory, Dec. 1972, pp. 23-35.

10. Leonard, Donald A.: Using Lasers to Monitor Stack Emissions. Instr. Control Systems, vol. 45, no. 8, Aug. 1972, pp. 73-76.

11. Melfi, S. H.; Brumfield, M. L.; and Storey, R. W., Jr.: Observation of Raman Scattering by SO_2 in a Generating Plant Stack Plume. Appl. Phys. Lett., vol. 22, no. 8, Apr. 15, 1973, pp. 402-403.

12. Cooney, John: Satellite Observation Using Raman Component of Laser Backscatter. Proceedings of the Symposium of Electromagnetic Sensing of the Earth from Satellites. Ralph Zirkind, ed., Polytechnic Institute of Brooklyn Press, 1967, pp. P1-P10.

14

13. Coney, T. A.; and Salzman, J. A.: Determination of the Temperature of Gas Mixtures by Using Laser Raman Scattering. NASA TN D-7126, 1973.

14. Hickman, R. S.; Liang, L. H.: Rotational Temperature Measurement in Nitrogen Using Raman Spectroscopy. Rev. Sci. Instr., vol. 43, no. 5, May 1972, pp. 796-799.

15. Lapp, Marshall; Penney, Carl M.; and St. Peters, Richard L.: Laser Raman Probe for Flame Temperature. SQUID-TR-GE-1-PU, Project Squid, Purdue Univ. (AD-759386), 1973.

16. Leser, Robert J.; and Salzman, Jack A.: Light Detection Electronics for a Raman Lidar. NASA TN D-6879, 1972.

17. Salzman, Jack A.; Masica, William J.; and Coney, Thom A.: Determining Gas Temperatures from Laser Scattering. Instruments and Control Systems, May 1972, pp. 67-71.

18. Pidgeon, C. R.: and Smith, S. D.: Resolving Power of Multilayer Filters in Nonparallel Light. Jour. Optical Soc. Amer., vol. 54, no. 12, Dec. 1962, pp. 1459-1466.

19. Krishnaw, Damala S.; Evans, William E.; Honey, Richard C.; and Sorenson, Glen P.: Development of a Turbidity Measuring Underwater Optical Radar System. Stanford Research Institute (AD-701416), 1969.

20. Cook, C. S.; and Bethke, G. W.: Design Construction and Evaluation of a Mobile Lidar System for the Remote Measurement of Smoke Plume Opacity. APTD-0968, General Electric Company (PB-210672), 1971.

21. Penney, C. M.; St. Peters, R. L.; and Lapp, M.: Absolute Intensity and Polarization of Rotational Raman Scattering from N_2, O_2, and CO_2. SRD-72-163, General Electric Co. (NASA CR-121091) 1973.

TABLE I. - FILTER PAIR TRANSMITTANCE CHARACTERISTICS

TABLE I. - FILTER PAIR TRANSMITTANCE CHARACTERISTICS

YIELDING MINIMUM STANDARD DEVIATION OF

TEMPERATURE MEASUREMENT CALCULATED

FOR TEMPERATURES NEAR 253 K

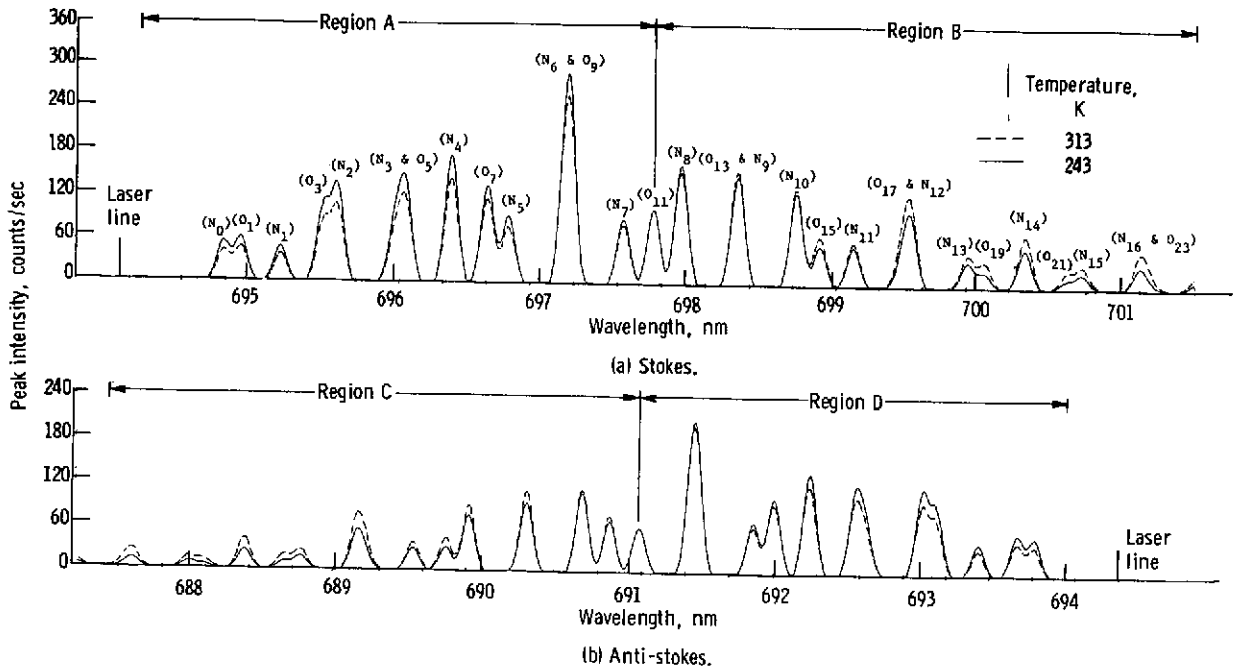| Transmittance characteristics, $I_{filter\ 1}/I_{filter\ 2}$	Standard deviation of temperature, K
$I_{687.8-2.8}/I_{696.2-0.8}$	7.90
$I_{687.8-2.6}/I_{692.6-0.8}$	8.71
$I_{696.2-0.8}/I_{701.4-2.9}$	8.80
$I_{692.6-0.8}/I_{701.4-2.7}$	9.76

Figure 1. - Comparison of theoretical Raman spectrum of air for temperatures of 243 and 313 K (incident laser wavelength at 694.3 nm).

16
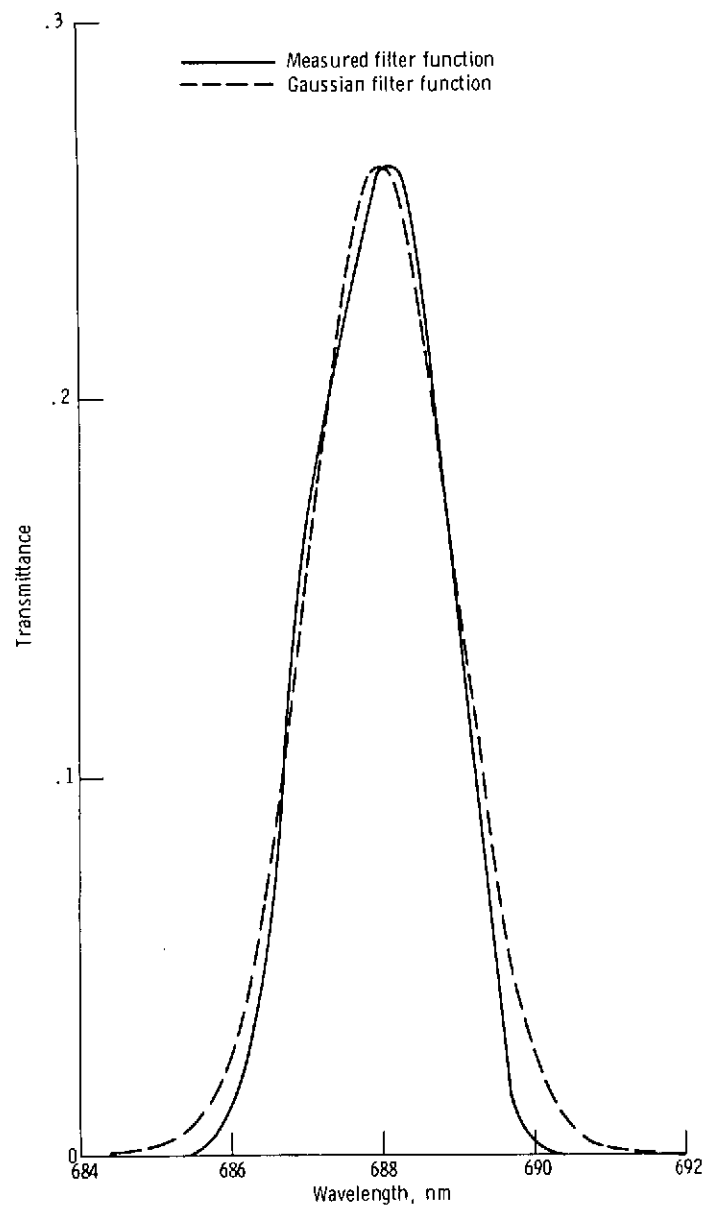
Figure 2. - Comparison of Gaussian and measured filter functions.
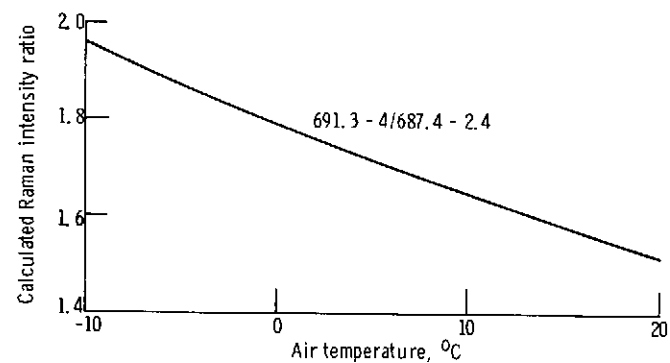
Figure 3. - Raman intensity ratio as function of temperature for typical filter pair.
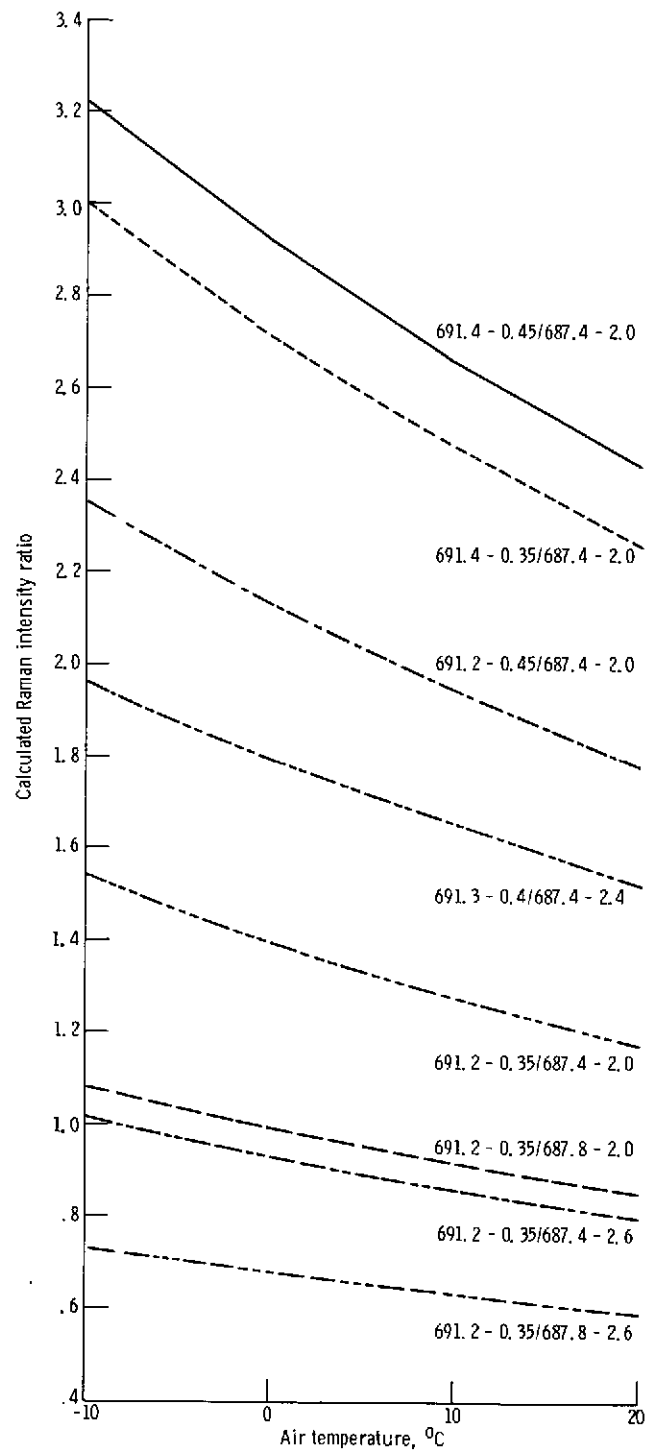
Figure 4. – Comparison of Raman intensity-ratio – temperature curves for various filter pairs.

691.4 - 0.45/687.4 - 2.0

691.4 - 0.35/687.4 - 2.0

691.2 - 0.45/687.4 - 2.0

691.3 - 0.4/687.4 - 2.4

691.2 - 0.35/687.4 - 2.0

691.2 - 0.35/687.8 - 2.0

691.2 - 0.35/687.4 - 2.6

691.2 - 0.35/687.8 - 2.6

Air temperature, °C

Calculated Raman intensity ratio
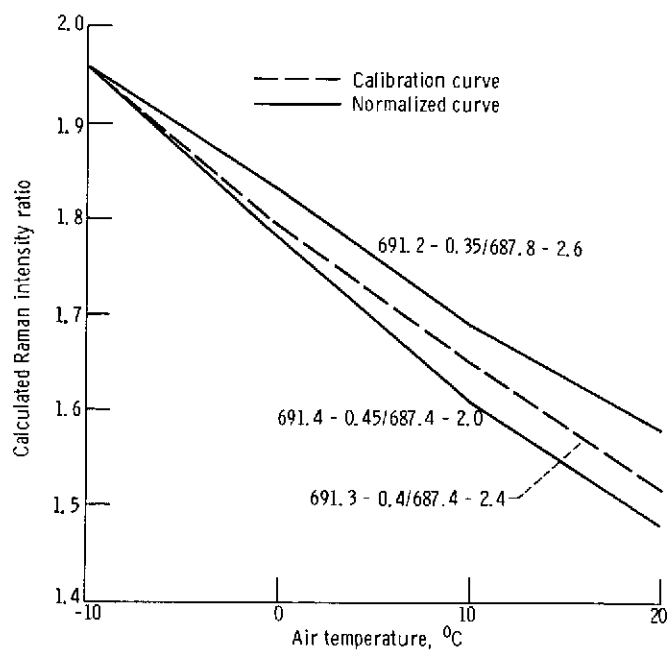
Figure 5. - Normalized curves for three filter pairs.
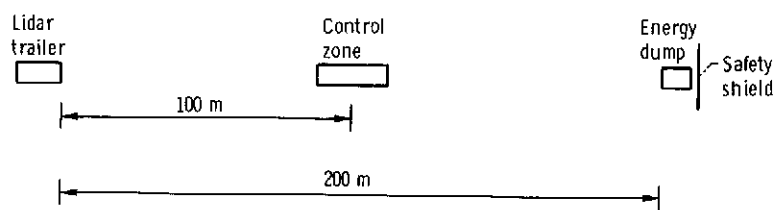
Figure 6. - Lidar test area.
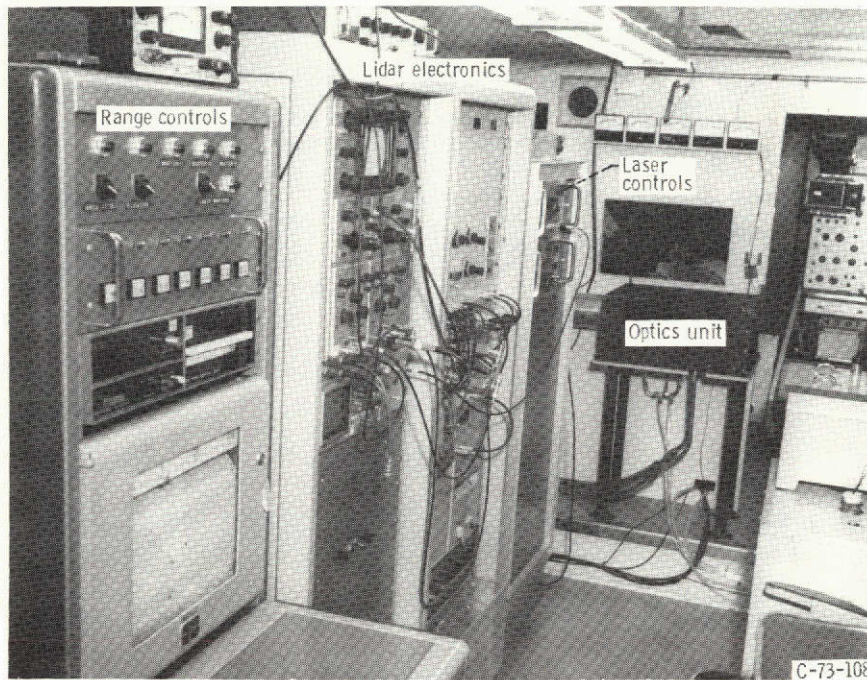
Figure 7. - Interior of lidar trailer.
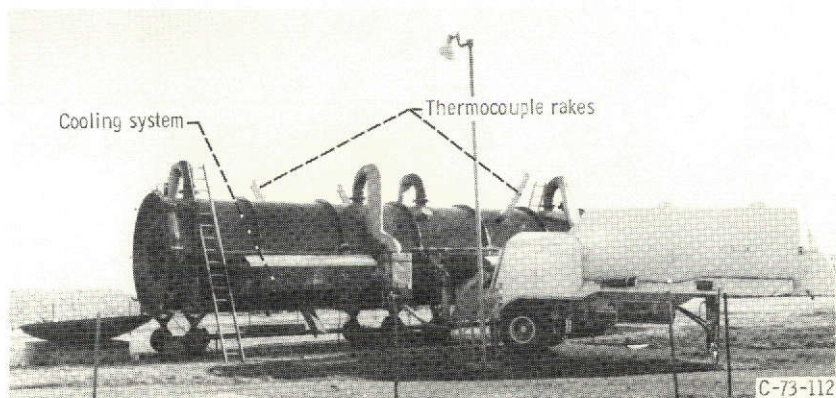
Figure 8. - Temperature control zone.
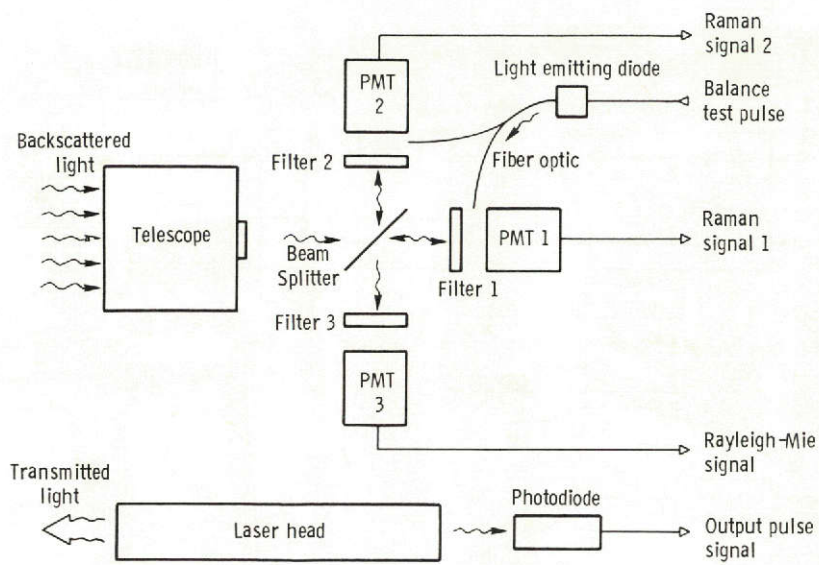
Figure 10. – Optical design schematic.
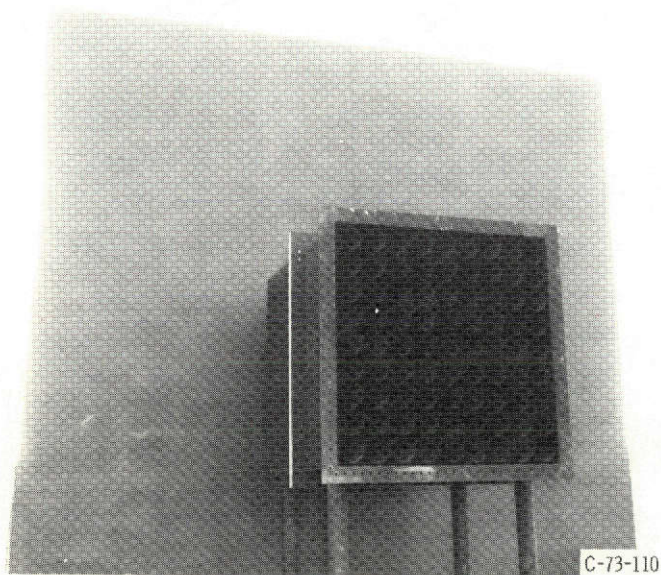
Figure 9. – Energy collector and safety shield.

Oscilloscopes

PMT 3

Numeric
display

Amplifiers

PMT 1   Amplifiers   Sample
gates   ADC'S   Printer

PMT 2

PMT
control

Start synchro-
nization   Range
control

Laser
control

Laser   Oscilloscope
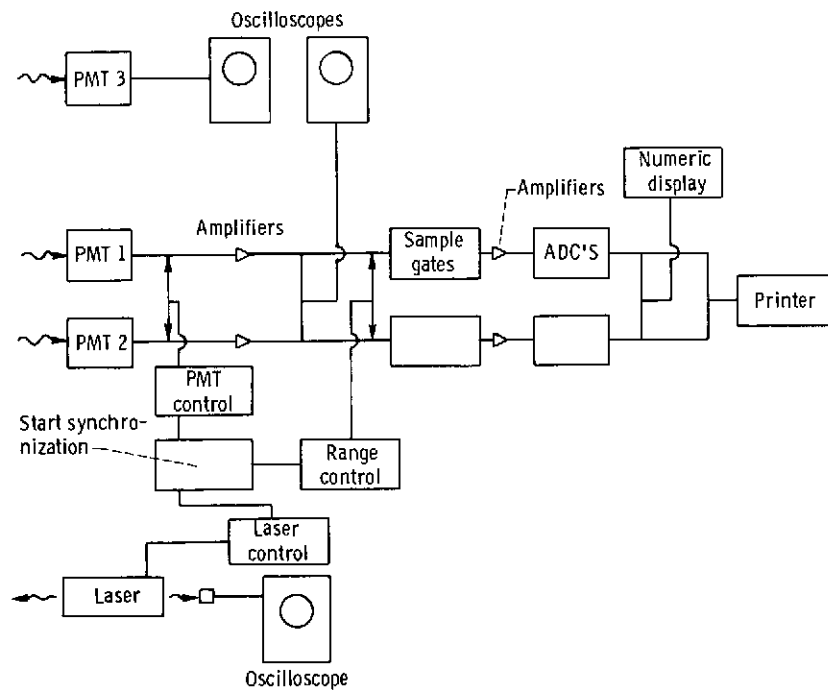
Figure 11. – Block diagram of lidar electronics.

Rayleigh-Mie channel

Raman channel 1

Relative signal intensity

Raman channel 2

0   100   200   300
Range, m
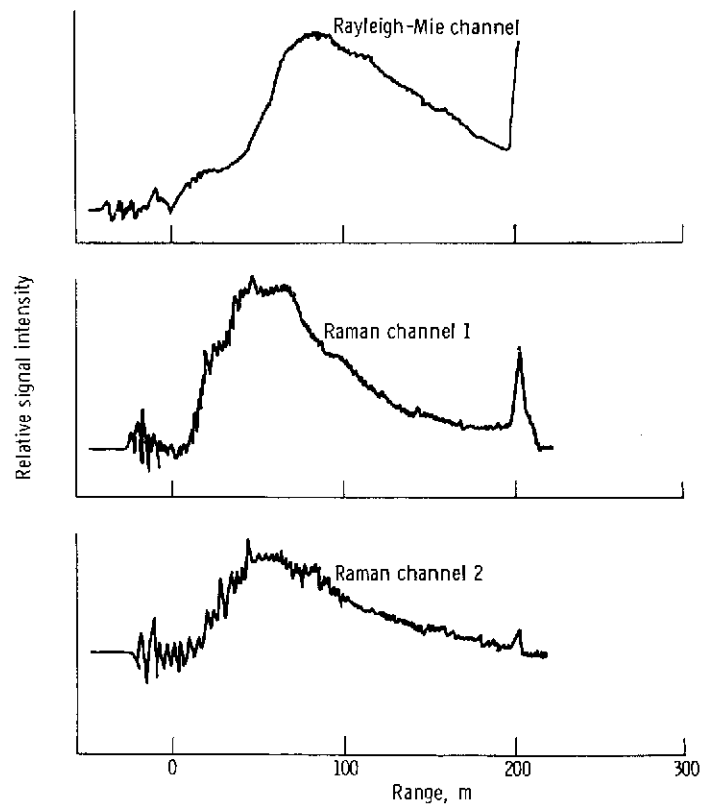
Figure 12. – Typical analog return signals.

22
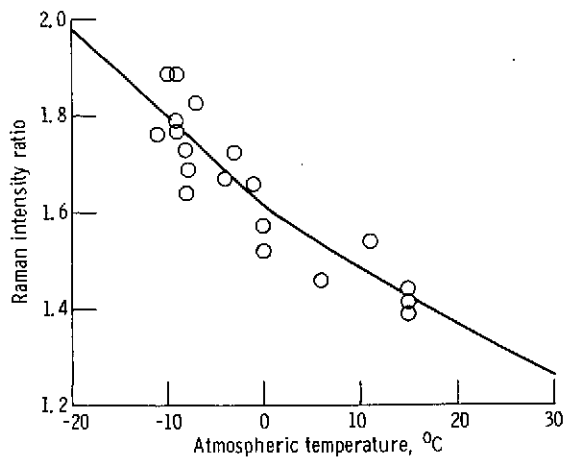
Figure 13. – Variation of Raman intensity ratio as function of ambient atmospheric temperature.
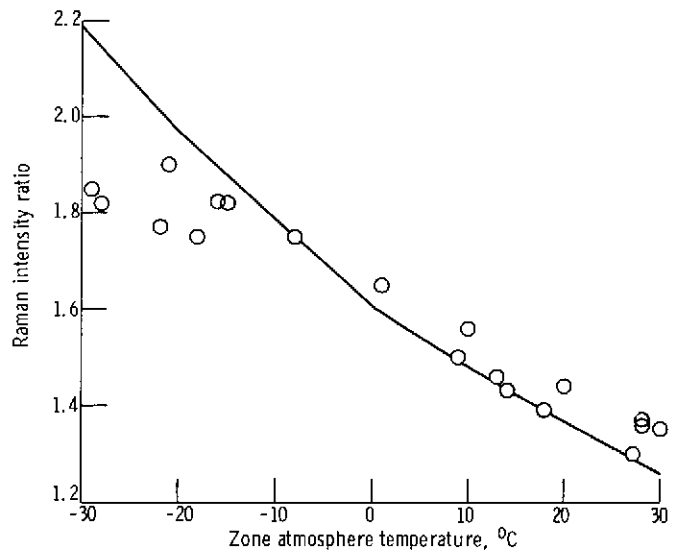
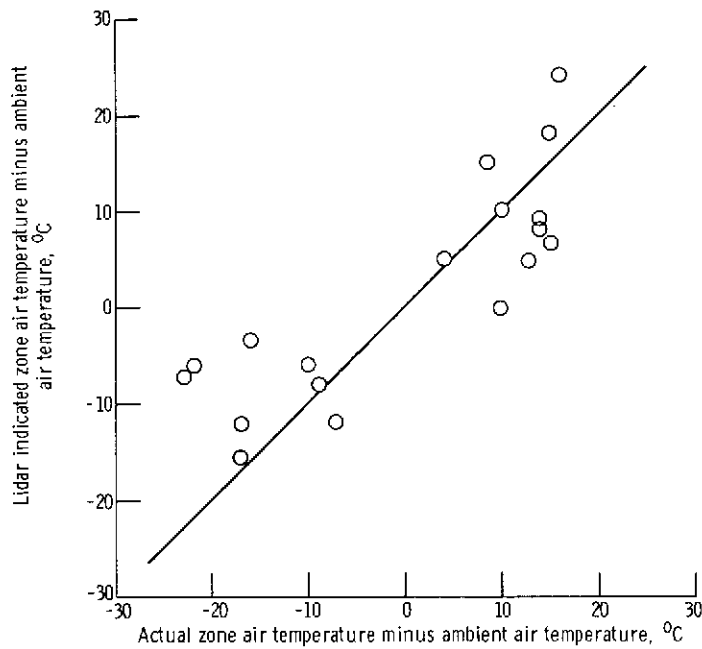Figure 14. – Measurement of temperature within the control zone.

Figure 15. – Measurement of difference between control zone air temperature and ambient air temperature.
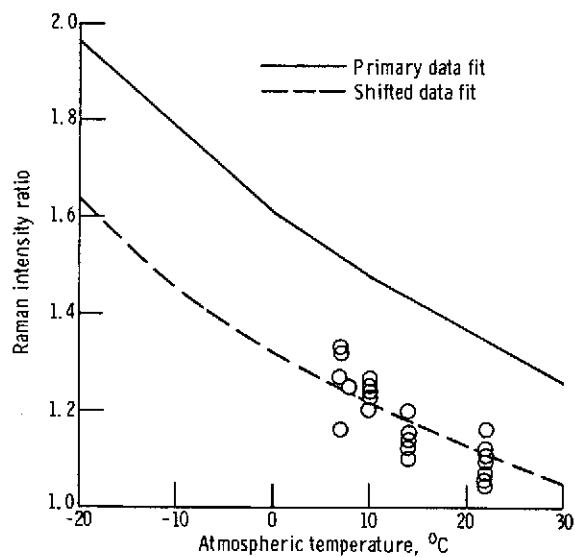
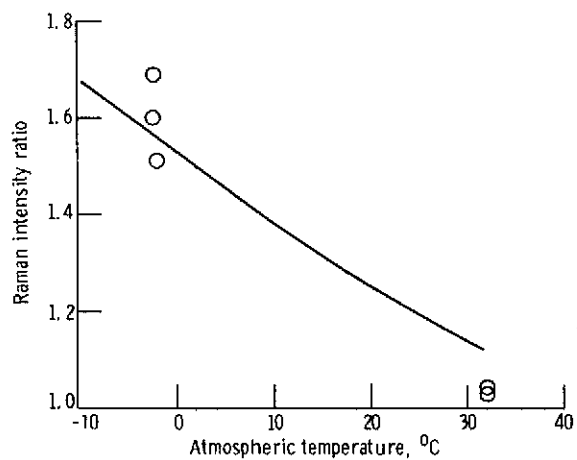Figure 16. - Ambient temperature data after change in filter function.

Figure 17. - Ambient temperature data with replacement filter combination.